JOURNAL OF THE MECHANICAL BEHAVIOR OF BIOMEDICAL MATERIALS 29 (2014) 663–675

Available online at www.sciencedirect.com

ScienceDirect

www.elsevier.com/locate/jmbbm

Research Paper

A one-dimensional mixed porohyperelastic transport swelling finite element model with growth

J.L. Harper[a], B.R. Simon[a,b], J.P. Vande Geest[a,b,c,d,*]

[a]Department of Aerospace and Mechanical Engineering, University of Arizona, United States
[b]Graduate Interdisciplinary Program in Biomedical Engineering, University of Arizona, United States
[c]Department of Biomedical Engineering, University of Arizona, United States
[d]Bio5 Institute for Biocollaborative Research, University of Arizona, United States

ARTICLE INFO

Article history:
Received 5 January 2013
Received in revised form
24 April 2013
Accepted 26 April 2013
Available online 7 May 2013

Keywords:
Finite elements
Porohyperelastic
Growth
Remodeling

ABSTRACT

A one-dimensional, large-strain, mixed porohyperelastic transport and swelling (MPHETS) finite element model was developed in MATLAB and incorporated with a well-known growth model for soft tissues to allow the model to grow (increase in length) or shrink (decrease in length) at constant material density. By using the finite element model to determine the deformation and stress state, it is possible to implement different growth laws in the program in the future to simulate how soft tissues grow and behave when exposed to various stimuli (e.g. mechanical, chemical, or electrical). The essential assumptions needed to use the MPHETS model with growth are clearly identified and explained in this paper. The primary assumption in this work, however, is that the stress upon which growth acts is the stress in the solid skeleton, i.e. the effective stress, S^{eff}. It is shown that significantly different amounts of growth are experienced for the same loading conditions when using a porohyperelastic model as compared to a purely solid model. In one particular example, approximately 51% less total growth occurred in the MPHETS model than in the solid model even though both problems were subjected to the same external loading. This work represents a first step in developing more sophisticated models capable of capturing the complex mechanical and biochemical environment in growing and remodeling tissues.

1. Introduction

The mechanics of hydrated soft tissues, including the deformation, stress, fluid pressure, fluid flux, and mobile species flux, are important to understand their function and behavior. While numerical models have been developed to simulate the immediate response of soft tissues to various conditions, the growth of the soft tissue over the long term is often neglected. A need exists to develop a soft tissue model which incorporates the ability of living biological tissues to grow and adapt to environmental changes or to medical device implantations. The work presented in this paper attempts to provide another step towards creating a more realistic model for describing the mechanical behavior and growth of complex soft tissues. In so doing, the knowledge base for understanding the biomechanics and pathophysiological phenomena of the body may be advanced leading to a more efficient means of disease diagnosis and treatment.

*Corresponding author at: Department of Aerospace and Mechanical Engineering, University of Arizona, United States. Tel.: +1 520 621 2514.
E-mail address: jpv1@email.arizona.edu (J.P. Vande Geest).

1751-6161/$ - see front matter © 2013 Elsevier Ltd. All rights reserved.
http://dx.doi.org/10.1016/j.jmbbm.2013.04.019

1.1. *Modeling of multiphasic soft tissues*

Many biological tissues consist of a porous solid skeleton saturated by an interstitial fluid in which a mobile species is dissolved. Soft hydrated biological tissues can experience large deformations, transport of the mobile fluid, as well as mechanical–chemical effects associated with the mobile species. A first approximation of the mechanical behavior of such materials may be seen in the early work of Biot (1941, 1972) and Bowen (1971a,b) in soils and geomechanics. Their work in describing porous rocks and soils provided the theoretical background for the application of these methods to biomechanics. As a result, general theoretical, numerical, and experimental multiphasic mixture/porous media models for hydrated soft tissues have been described in numerous papers (Vande Geest et al., 2011; Almeida and Spilker, 1997, 1998; Gu et al., 1998; Lai et al., 1991; Simon et al., 1998a,b; Spilker et al., 1992). In order to provide numerical solutions to the highly nonlinear, coupled, initial boundary value problems which occur in soft tissue mechanics, various finite element models (FEMs) based on a continuum mixture view (or an equivalent continuum porous media view) of these materials have been developed. Several (Simon et al., 1998a; Levenston et al., 1998; Iatridis et al., 2003) have simulated the complex response of hydrated soft tissues by considering poroelastic solids saturated with mobile fluid and multiple charged mobile species using continuum models and their corresponding FEMs. There exists a need to connect these FEMs with growth and remodeling theory.

1.2. *Growth and remodeling*

Unlike traditional engineering materials, biological soft tissues possess the ability to change their shape and behavior in response to environmental changes such as electrical, chemical, or mechanical stimuli. Exactly how to model this growth, however, remains an open question in the field of biomechanics as "different approaches exist to model relationships between changes in mass, kinematics, the origin of residual stress, the evolution of natural configurations of a growing body or its constituent parts, and other associated aspects of growth" (Ambrosi et al., 2011). One common approach has been to decompose the deformation gradient tensor into elastic and growth components; the coupled solution of balances of mass and linear momentum then governs changes in form can successfully model residual stress in growing tissues (Ambrosi et al., 2011). Another general approach has been to incorporate biologically driven mass density productions and survival functions within constitutive relations for stress response based on simple rule of mixture formulations (Humphrey and Rajagopal, 2002; Ambrosi et al., 2011).

While some controversy exists about the appropriateness of each method, many agree that it would be beneficial to incorporate growth with "mixture theory so as to include contributions of diverse constituents (solid and fluid as well as electrolytes, growth factors and cytokines, and nutrients and waste products within the interstitial fluid) involved in the underlying biochemical and biophysical processes" (Ambrosi et al., 2011). For example, Ateshian (2007) provides one view point of modeling growth with mixture theory by requiring the mechanisms of growth to explicitly satisfy the conservation of mass of the fluid and solid constituents. Regardless of the approach for modeling growth and remodeling, it is clear that incorporation of such theoretical formulations into computational models that can account for solid, fluid, and biochemical phenomena is warranted.

1.3. *Objective*

The objectives of this paper are two-fold. The first objective is to develop in MATLAB a one-dimensional, large-strain, mixed porohyperelastic transport and swelling (MPHETS) finite element model which may be used to accurately model hydrated soft tissues. The second objective is to incorporate this model with a well-known growth model for soft tissues. While our choice of the specific model for growth is based on its long standing use by many in the literature, our approach can easily be modified implement different growth laws as deemed appropriate in future work. Since the key assumption for implementing the representative growth law chosen here is that the stimulus for growth is stress, we will compare and contrast how the results from such a chosen model vary when the growth law is stimulated by the effective stress, S^{eff}, in our MPHETS model. The influence of osmotic swelling effects will also be explored. By accomplishing the above, a first step will be made towards creating future models in which growth occurs in response to more complex biomechanical and biochemical stimuli (e.g., interstitial flows, concentrations of dissolved species).

2. Methods

2.1. *Assumptions and conventions*

The MPHETS theory presented here employs an incompressible hyperelastic porous solid skeleton that is fully saturated by an incompressible mobile fluid that is free to displace relative to the solid skeleton. The pores are considered to be sufficiently small such that the solid may be viewed as a continuum with a known porosity and permeability. Any displacement of the solid must be accompanied by a corresponding movement of the fluid into or out of the solid. Since this work is only concerned with a one-dimensional model, the cross-sectional area is assumed to remain constant at all times. Additionally, temperature is also assumed to remain constant.

2.2. *Conventions*

In this paper, the following conventions will be used:

(1) A tilde (˜) is used to denote a Lagrangian quantity.
(2) A bar "¯" above a non-superscript or non-subscript quantity denotes a nodal solution variable.
(3) The superscripts "s", "f", and "c" above a quantity denote a solid, fluid, and species quantity, respectively.
(4) A subscript "o" denotes an initial quantity.
(5) A superscript "g" denotes a quantity that is to be evaluated at the Gauss point of the finite element.

(6) As this paper is posed in one dimension, the one–one position of a tensorial variable will be denoted as the variable without indices. For example, the one-dimensional form of F_{ij} will be F.

2.3. *Governing equations for porohyperelastic mass transport-swelling*

2.3.1. *Kinematics*

For a thorough description of the MPHETS theory the reader is referred to Kaufmann (1996) and Vande Geest et al. (2011). An abbreviated version is provided here. An initial volume of material dV_0 is located at some reference position X_i at initial time t_0. At time t, following deformation, the volume becomes dV located at position x_i. The volumetric deformation is captured by

$$J = \frac{dV}{dV_0}. \tag{1}$$

Assuming that the porous media is fully saturated by the incompressible mobile fluid, the porosity of the material, n, may be defined as the ratio of the fluid volume to the total volume and is given by

$$n = \frac{dV^f}{dV} \tag{2}$$

where

$$dV = dV^s + dV^f. \tag{3}$$

Note that the total volume of the dissolved mobile species is neglected. The initial porosity at time t_0 is defined as

$$n_0 = \frac{dV_0^f}{dV_0} \tag{4}$$

where

$$dV_0 = dV_0^s + dV_0^f \tag{5}$$

Since the solid is incompressible it follows that

$$dV^s = dV_0^s. \tag{6}$$

The porosity can be expressed as a function of the deformation by

$$J = \frac{dV}{dV_0} = \frac{dV^s + dV^f}{dV_0} = \frac{dV_0^s}{dV_0} + \frac{dV^f}{dV_0} = (1-n_0) + Jn \tag{7}$$

which can be rearranged as

$$n = 1 - J^{-1}(1-n_0). \tag{8}$$

Note that Eqs. (6)–(8) are only valid if growth has not yet occurred, i.e. if mass has not been added to the solid skeleton. Although both the solid skeleton and the fluid are assumed to be incompressible, the total material is compressible due to a net gain or loss of fluid volume. The displacement of the solid is given by

$$u_i = x_i - X_i \tag{9}$$

with the associated material time derivatives

$$\dot{u}_i = v_i^s = \frac{du}{dt} \tag{10}$$

$$\dot{u}_i = \frac{d\dot{u}_i}{dt}. \tag{11}$$

The deformation gradient is given by

$$F_{ij} = \frac{\partial x_i}{\partial X_j}. \tag{12}$$

The engineering strain, Green's strain, and Finger's strain are, respectively, given by

$$e_{ij} = \frac{1}{2}\left(\frac{\partial u_i}{\partial X_j} + \frac{\partial u_j}{\partial X_i}\right) \tag{13}$$

$$E_{ij} = \tfrac{1}{2}(F_{li}F_{lj} - \delta_{ij}) \tag{14}$$

$$H_{ij} = F_{im}^{-1}F_{jm}^{-1}. \tag{15}$$

Note that the volume strain of the material can also be expressed as

$$J = \det(F_{ij}). \tag{16}$$

The velocity strain is

$$D_{ij} = \frac{1}{2}\left(\frac{\partial v_i}{\partial x_j} + \frac{\partial v_j}{\partial x_i}\right) \tag{17}$$

which, when combined with the dilatational velocity strain

$$D_{kk} = \frac{\partial v_k}{\partial x_k} = \frac{\dot{J}}{J} \tag{18}$$

and the increment/rate of Jn

$$\frac{d}{dt}(Jn) = \dot{J} \tag{19}$$

allows $\dot{J}$ to be expressed as

$$\dot{J} = JD_{kk}. \tag{20}$$

The rate of deformation (velocity strain), Green's strain, and the volume strain are related by

$$\dot{E}_{ij} = F_{ki}D_{km}F_{mj} \tag{21}$$

$$\dot{J} = JD_{kk} = J\dot{E}_{rs}H_{rs}. \tag{22}$$

The rate of change of Finger's strain is

$$\dot{H}_{ij} = -2H_{ik}H_{jl}\dot{E}_{kl}. \tag{23}$$

The displacement of the fluid at a point, u_i^f, is defined in an *average* sense such that the volume of fluid that is displaced through a unit area perpendicular to an axis is given as nu_i^f. Using this definition, the apparent relative fluid velocity is defined as the average fluid velocity relative to the deforming solid as

$$v_i^{fr} = n(v_i^f - v_i^s) \tag{24}$$

Note that the apparent relative fluid velocity is also the apparent relative fluid flux. Similarly, the apparent relative mobile species velocity is

$$v_i^{cr} = n(v_i^c - v_i^s) \tag{25}$$

with the apparent relative mobile species flux being

$$j_i^{cr} = cv_i^{cr} = cn(v_i^c - v_i^s). \tag{26}$$

Note that the species is considered to be dissolved in the fluid so that the species concentration is defined in terms of the

fluid volume and the number of moles of the species, dm^c, as

$$c = \frac{dm^c}{dV^f} \tag{27}$$

where c has units of moles per cubic meter of interstitial fluid. The relative volumetric fluid strain rate is

$$D^{fr}_{kk} = \frac{\partial v^{fr}_k}{\partial x_k} \tag{28}$$

which in Lagrangian form can be expressed as

$$\tilde{D}^{fr}_{kk} = JD^{fr}_{kk}. \tag{29}$$

2.3.2. Conservation equations

The three conservation equations used in the porohyperleastic mass transport theory are described below.

(1) *Conservation of linear momentum*: The Lagrangian conservation of momentum is:

$$\frac{\partial T_{ji}}{\partial X_j} + J\rho b_i + \tilde{R}^s_i = 0 \tag{30}$$

where T_{ij} is the total Lagrangian stress (force per unit area), ρ is the density of the material, b_i are the body forces applied to the material, and $\tilde{R}^s_i$ is the solid source term. In the absence of body forces or source terms, the Lagrangian conservation of momentum may be reduced to the form that is used in this work

$$\frac{\partial T_{ji}}{\partial X_j} = 0 \text{ or in its one} - \text{dimensional form } \frac{\partial T}{\partial X} = 0 \tag{31}$$

Note that if body forces were included, then a follower loading capability could be implemented and demonstrated.

(2) *Conservation of mass (for the incompressible fluid and solid)*: The general conservation of mass equation is

$$\frac{\partial \rho}{\partial t} + \frac{\partial \rho v_i}{\partial x_i} + R^s_i = 0 \tag{32}$$

which without source terms and at steady state becomes

$$\frac{\partial \rho v_i}{\partial x_i} = 0. \tag{33}$$

Since both the fluid and solid have constant density and are incompressible, this simplifies to

$$\frac{\partial v_i}{\partial x_i} = 0. \tag{34}$$

For a section of material, v may be split into fluid and solid proportions via the porosity as

$$v_i = nv^f_i + (1-n)v^s_i. \tag{35}$$

Solving Eq. (24) for v^f_i and substituting the result into Eq. (35) yields

$$v_i = v^{fr}_i + v^s_i. \tag{36}$$

Eq. (34) can then be rewritten as

$$\frac{\partial (v^{fr}_i + v^s_i)}{\partial x_i} = \frac{\partial v^{fr}_i}{\partial x_i} + \frac{\partial v^s_i}{\partial x_i} = 0. \tag{37}$$

which after use of Eq. (18) becomes

$$\frac{\partial v^{fr}_i}{\partial x_i} + D_{kk} = 0. \tag{38}$$

Using Eqs. (20), (22), (29), and (38), the Lagrangian conservation of mass for the incompressible solid and mobile incompressible fluid without source terms may finally be expressed as

$$\frac{\partial \tilde{v}^{fr}_i}{\partial X_i} + \dot{J} = \frac{\partial \tilde{v}^{fr}_i}{\partial X_i} + JH_{ij}\dot{E}_{ij} = \frac{\partial \tilde{j}^{fr}_i}{\partial X_i} + JH_{ij}\dot{E}_{ij} = 0 \tag{39}$$

Which in one-dimension becomes

$$\frac{\partial \tilde{j}^{fr}}{\partial X} + JH\dot{E} = 0 \tag{40}$$

(3) *Conservation of mass (for the neutral mobile species)*: The general conservation of mass equation for the neutral mobile species is

$$\frac{\partial \rho^c}{\partial t} + \frac{\partial \rho^c v^{cr}_i}{\partial x_i} + R^c_i = 0 \tag{41}$$

which without source terms becomes

$$\frac{\partial \rho^c}{\partial t} + \frac{\partial \rho^c v^{cr}_i}{\partial x_i} = 0. \tag{42}$$

Since $\rho^c = nc$, this may be written as

$$\frac{\partial nc}{\partial t} + \frac{\partial ncv^{cr}_i}{\partial x_i} = 0 \tag{43}$$

or

$$\frac{\partial c}{\partial t} + \frac{\partial cv^{cr}_i}{\partial x_i} = \frac{\partial c}{\partial t} + \frac{\partial j^{cr}_i}{\partial x_i} = 0. \tag{44}$$

In the Lagrangian form, this becomes

$$\frac{\partial \tilde{j}^{cr}_i}{\partial X_i} + \dot{\tilde{c}} = 0 \tag{45}$$

where

$$\tilde{c} = Jnc. \tag{46}$$

Note that

$$c = c(x,t) = c(X,t) \tag{47}$$

with the subtle difference that

$$\tilde{c} = Jnc = \tilde{c}(X,t) \neq c(X,t). \tag{48}$$

Using these definitions, Eq. (45) becomes

$$\frac{\partial \tilde{j}^{cr}_i}{\partial X_i} + \frac{d(Jn)}{dt}c + Jn\dot{c} = 0. \tag{49}$$

With Eqs. (19) and (22) this can be rewritten

$$\frac{\partial \tilde{j}^{cr}_i}{\partial X_i} + JH_{ij}\dot{E}_{ij}c + Jn\dot{c} = 0 \tag{50}$$

which has a one-dimensional form of

$$\frac{\partial \tilde{j}^{cr}}{\partial X} + cJH\dot{E} + Jn\dot{c} = 0. \tag{51}$$

2.3.3. MPHETS constitutive equations

The three constitutive equations required in the MPHETS theory are the effective stress principle and the two Onsager

equations (see Vande Geest et al., 2011). The prior requires the definition of an effective strain energy density.

(1) *Effective stress principle*: The porous medium consists of a solid and a fluid component. The stress at any point within the medium is decomposed into an effective stress and a pore fluid pressure as

$$\sigma_{ij} = \sigma_{ij}^{eff} - p^f \delta_{ij} \tag{52}$$

where σ_{ij} is the Cauchy stress, σ_{ij}^{eff} is the effective Cauchy stress, and p^f is the mechanical pore fluid pressure. Since the 2nd Piola-Kirchhoff S_{ij} stress can be related to the Cauchy stress by

$$S_{ij} = JF_{im}^{-1}\sigma_{mk}F_{jk}^{-1} \tag{53}$$

we can write

$$S_{ij} = S_{ij}^{eff} - JH_{ij}p^f \tag{54}$$

where S_{ij} is the total 2nd Piola-Kirchhoff stress and S_{ij}^{eff} is the effective 2nd Piola-Kirchhoff stress. The total nominal stress can then be calculated as

$$T_{ij} = F_{ik}S_{kj} = F_{ik}(S_{kj}^{eff} - JH_{kj}p^f) \tag{55}$$

which in one-dimension becomes

$$T = FS = F(S^{eff} - JHp^f) \tag{56}$$

where

$$S = S^{eff} - JHp^f. \tag{57}$$

(2) *Onsager equations*: The rate of flow of the fluid and the flux of the species relative to the porous medium can be written using coupled Onsager equations. The Lagrangian forms of these equations are, respectively,

$$\tilde{j}_i^{fr} = \tilde{v}_i^{fr} = -\tilde{L}_{ij}^{ff}e_j^{f^*} - \tilde{L}_{ij}^{fc}e_j^{c^*} = -\tilde{L}_{ij}^{ff}\frac{\partial\tilde{\mu}^{f^*}}{\partial X_j} - \tilde{L}_{ij}^{fc}\frac{\partial\tilde{\mu}^{c^*}}{\partial X_j} \tag{58}$$

$$\tilde{j}_i^{cr} = c\tilde{v}_i^{cr} = -\tilde{L}_{ij}^{cf}e_j^{f^*} - \tilde{L}_{ij}^{cc}e_j^{c^*} = -\tilde{L}_{ij}^{cf}\frac{\partial\tilde{\mu}^{f^*}}{\partial X_j} - \tilde{L}_{ij}^{cc}\frac{\partial\tilde{\mu}^{c^*}}{\partial X_j} \tag{59}$$

where $\tilde{L}_{ij}^{ff}$, $\tilde{L}_{ij}^{fc}$, $\tilde{L}_{ij}^{cf}$, and $\tilde{L}_{ij}^{cc}$ are the Onsager coefficients and the potentials ($\tilde{\mu}^{f^*}$ and $\tilde{\mu}^{c^*}$) in Eqs. (58) and (59) are assumed to be independent of the deformation. The total fluid pressure, $\tilde{\mu}^{f^*}$, is described as the sum of the mechanical fluid pressure, p^f, and the osmotic fluid pressure, p^o. The electro-chemical potential, $\tilde{\mu}^{c^*}$, is the sum of an electrical potential, μ^{ce}, and a chemical potential, μ^c. However, for a single neutral species, $\mu^{ce}=0$. The potentials may then be determined as

$$\tilde{\mu}^{f^*}(X,t) = \mu^{f^*}(x,t) = p^f + p^o \tag{60}$$

$$\tilde{\mu}^{c^*}(X,t) = \mu^{c^*}(x,t) = \mu^c + \mu^{ce} = \mu^c = \tilde{\mu}^c \tag{61}$$

where

$$p^o = p_0^o - R\theta\phi^c c \tag{62}$$

$$\mu^c = \mu_0^c + R\theta\log(\gamma^c c). \tag{63}$$

The necessary transport properties that must be specified are the hydraulic permeability (k_{ij}^{ff}), the convection coupling coefficient ($b_{ij}^{cf} = b_{ij}^{fc}$), the diffusivity ($d_{ij}^{cc}$), the osmotic coefficient (ϕ^c), and the activity coefficient (γ^c). By making use of Darcy's Law, Fick's Law, and the definitions of the potentials, these transport properties can be related to the Onsager coefficients as follows:

$$L_{ij}^{ff} = k_{ij}^{ff} \tag{64}$$

$$L_{ij}^{cf} = cb_{ik}^{cf}k_{kj}^{ff} = k_{ik}^{ff}b_{kj}^{fc}c = L_{ij}^{fc} \tag{65}$$

$$L_{ij}^{cc} = \frac{c}{R\theta}d_{ij}^{cc} + cb_{il}^{cf}k_{lk}^{ff}b_{kj}^{fc}c. \tag{66}$$

In order to be used in the porous media theory, the Eulerian Onsager coefficients must be transformed to their Lagrangian forms as follows:

$$\tilde{L}_{ij}^{ff} = JH_{ik}L_{kj}^{ff} = JH_{ik}k_{kj}^{ff} \tag{67}$$

$$\tilde{L}_{ij}^{cf} = JH_{ik}L_{kj}^{cf} = cJH_{ik}b_{kl}^{cf}k_{lj}^{ff} = cJH_{ik}k_{kl}^{ff}b_{lj}^{fc} = JH_{ik}L_{kj}^{fc} = \tilde{L}_{ij}^{fc} \tag{68}$$

$$\tilde{L}_{ij}^{cc} = JH_{ik}L_{kj}^{cc} = J\frac{c}{R\theta}H_{ik}d_{kj}^{cc} + cJH_{im}b_{ml}^{cf}k_{lk}^{ff}b_{kj}^{fc}c. \tag{69}$$

In one-dimension, the Onsager equations and their respective properties become

$$\tilde{j}^{fr} = \tilde{v}^{fr} = -\tilde{L}^{ff}e^{f^*} - \tilde{L}^{fc}e^{c^*} = -\tilde{L}^{ff}\frac{\partial\tilde{\mu}^{f^*}}{\partial X} - \tilde{L}^{fc}\frac{\partial\mu^{c^*}}{\partial X} \tag{70}$$

$$j^{cr} = cv^{cr} = -\tilde{L}^{cf}e^{f^*} - \tilde{L}^{cc}e^{c^*} = -\tilde{L}^{cf}\frac{\partial\tilde{\mu}^{f^*}}{\partial X} - \tilde{L}^{cc}\frac{\partial\mu^{c^*}}{\partial X} \tag{71}$$

$$\tilde{L}^{ff} = JHL^{ff} = JHk^{ff} \tag{72}$$

$$\tilde{L}^{cf} = JHL^{cf} = JHcb^{cf}k^{ff} = JHk^{ff}b^{fc}c = JHL^{fc} = \tilde{L}^{fc} \tag{73}$$

$$\tilde{L}^{cc} = JHL^{cc} = JH\frac{c}{R\theta}d^{cc} + cb^{cf}k^{ff}b^{fc}c \tag{74}$$

It is important to note that in the present work, the Eulerian transport properties k^{ff}, b^{fc}, b^{cf}, and d^{cc} are assumed to be isotropic and constant.

3. *Strain energy density*: In order to demonstrate our approach, we chose here to utilize a simple Neo-Hookean strain energy density function. This form has been used by Kuhl (Himpel et al., 2005; Goktepe et al., 2010) and may be written as

$$\Psi = \tfrac{1}{2}\lambda\ln^2(J) + \tfrac{1}{2}\mu[C_{ij}\delta_{ji} - 3 - 2\ln(J)] \tag{75}$$

where C_{ij} is the right Cauchy-Green tensor. The 2nd Piola-Kirchhoff stress is then calculated as

$$\begin{aligned} S_{ij} &= \frac{\partial\Psi}{\partial E_{ij}} = 2\frac{\partial\Psi}{\partial C_{ij}} = \lambda\frac{\partial\ln^2(J)}{\partial C_{ij}} + \mu\frac{\partial(C_{ij}\delta_{ji})}{\partial C_{ij}} - 2\mu\frac{\partial\ln(J)}{\partial C_{ij}} \\ &= \lambda\frac{\partial\ln^2(J)}{\partial F_{ij}}\frac{\partial F_{ij}}{\partial C_{ij}} + \mu\frac{\partial(C_{ij}\delta_{ji})}{\partial C_{ij}} - 2\mu\frac{\partial\ln(J)}{\partial F_{ij}}\frac{\partial F_{ij}}{\partial C_{ij}} \\ &= \left[\lambda\frac{\partial\ln^2(J)}{\partial F_{ij}} - 2\mu\frac{\partial\ln(J)}{\partial F_{ij}}\right]\frac{\partial F_{ij}}{\partial C_{ij}} + \mu\frac{\partial(C_{ij}\delta_{ji})}{\partial C_{ij}} \\ &= [2\lambda\ln(J)(F_{ki})^{-1} - 2\mu(F_{ki})^{-1}]\left(\frac{1}{2}F_{lk}(C_{lj}^{-1})\right) + \mu\delta_{ij} \\ &= [\lambda\ln(J) - \mu](C_{ij}^{-1}) + \mu\delta_{ij} \end{aligned} \tag{76}$$

For flowing confined compression (which is used here), $J=F$, $E=\frac{1}{2}(F^2-1)$, and $C=F^2$ so Eq. (76) may be written as

$$S = [\lambda\ln(F) - \mu]F^{-2} + \mu \tag{77}$$

The incremental tangent modulus may now be determined by taking the increment/rate of Eq. (77)

$$\dot{S} = \left(\frac{2\mu}{F^3} - \frac{2\lambda \ln(F)}{F^3} + \frac{\lambda}{F^3}\right)\dot{F} = (2\mu - 2\lambda \ln(F) + \lambda)F^{-3}\dot{F} \tag{78}$$

If we consider Eq. (78) for when $F=1$:

$$\dot{S} = (2\mu + \lambda)\dot{F} = H_A\dot{F} \tag{79}$$

where H_A is the aggregate modulus. By writing Eq. (78) in the form of $\dot{S} = \tilde{H}_A\dot{E}$ or $\Delta S = \tilde{H}_A\Delta E$ where $\tilde{H}_A$ is the incremental tangent modulus and by using the fact that $\dot{E} = F\dot{F}$, the following is obtained

$$\dot{S} = (2\mu - 2\lambda \ln(F) + \lambda)F^{-4}\dot{E} \tag{80}$$

or

$$\Delta S = \tilde{H}_A \Delta E \tag{81}$$

where the incremental tangent modulus is defined as

$$\tilde{H}_A = (2\mu + \lambda - 2\lambda \ln(F))F^{-4}. \tag{82}$$

2.4. Governing equations for growth

2.4.1. Assumptions

The growth theory utilized here will follow closely the work of Kuhl (Himpel et al., 2005; Goktepe et al., 2010) and as such attends to growth at the kinematic level. It will be assumed in this model that growth is stress-based and that other factors which may contribute to the growth of a soft tissue (i.e. the concentration of a mobile species, etc.) can currently be neglected. It is important to note, however, that growth factors other than stress may be implemented into the model in the future and that different growth laws may be used in place of the one chosen here. Finally, it must be noted that the stress upon which the growth loop will act is the stress in the solid skeleton, i.e. the effective stress, S^{eff}. The reader should note that the stresses used in the following growth theory refers to the effective stress from the above described MPHETS theory.

2.4.2. Growth kinematics

Within the framework of finite growth, the key kinematic assumption is the multiplicative decomposition of the deformation gradient F_{ij} into an elastic part F^e_{ij} and a growth part F^g_{ij}:

$$F_{ij} = F^e_{ik}F^g_{kj}. \tag{83}$$

This concept was first proposed by Lee (1969) in the context of finite elasto-plasticity and was later applied in the context of growth by Rodriguez and Hoger (1994); it has also been adopted by Kuhl amongst others (Himpel et al., 2005; Goktepe et al., 2010; Ambrosi et al., 2011; Ambrosi and Mollica, 2002). This decomposition can be depicted as shown in Fig. 1.

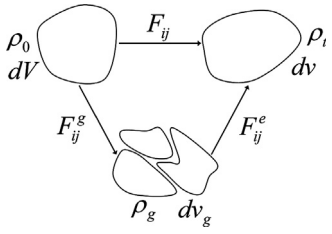

Fig. 1 – Multiplicative decomposition of the deformation gradient.

As illustrated, the body is initially at volume dV and density ρ_0. The deformation of the body due to growth will now be decomposed into two parts. First, every particle of the body will grow or decrease in mass under a stress free condition. This growth part of the deformation, denoted by F^g_{ij}, results in an intermediate configuration where the body has volume dv_g and density ρ_g. Since the grown body may not be compatible at this point, an additional elastic deformation, denoted by F^e_{ij}, may be necessary to ensure the compatibility of the total deformation. Once this second part of the deformation has occurred, the body is now in its final grown state (known as the spatial configuration) with volume dv and density ρ_t. Again, note that the total deformation of the body due to growth can be computed by $F_{ij} = F^e_{ik}F^g_{kj}$. The theory presented in the rest of this chapter is based on the work done by Lubarda and Hoger (2002) and Kuhl (Himpel et al., 2005; Goktepe et al., 2010). At this point, let us define the right Cauchy-Green tensor and the elastic right Cauchy-Green tensor as

$$C_{ij} = F_{ki}F_{kj} \tag{84}$$

$$C^e_{ij} = F^e_{ki}F^e_{kj} \tag{85}$$

And the spatial velocity gradient and the growth velocity gradient as

$$L_{ij} = \frac{\partial v_i}{\partial x_j} = \dot{F}_{ik}F^{-1}_{kj} \tag{86}$$

$$L^g_{ij} = \frac{\partial v^g_i}{\partial x_j} = \dot{F}^g_{ik}(F^g_{kj})^{-1} \tag{87}$$

In analogy to the Jacobian $J = \det(F_{ij})$ of the total deformation gradient, we may define the Jacobians of the growth deformation gradient and the elastic deformation gradient, respectively, as

$$J^g = \det(F^g_{ij}) \tag{88}$$

$$J^e = \det(F^e_{ij}). \tag{89}$$

Also note that we may write

$$J = \det(F_{ij}) = \det(F^e_{ik}F^g_{kj}) = J^eJ^g. \tag{90}$$

Using the above definitions, the following well-known relations may be written:

$$dv = J\,dV \tag{91}$$

$$dv_g = J^g\,dV \tag{92}$$

$$dv = J^e\,dv_g \tag{93}$$

and the initial mass element may be obtained as

$$dM = \rho_0\,dV. \tag{94}$$

By denoting R_0 as a mass source per unit volume term in the material configuration and by neglecting any mass flux through the surface of the element under consideration, the grown mass element dm will consist of the initial mass element dM and the additional mass produced by the mass source term R_0 during the time interval $[t_0, t]$. This may be

calculated as

$$dm = dM + \int_{t_0}^{t} R_0 \, dt \, dV \tag{95}$$

In the intermediate configuration, the mass element may also be written as

$$dm = \rho_g \, dv_g \tag{96}$$

Since the deformation map between the intermediate configuration and the spatial configuration is a purely elastic map, the mass element expressed in terms of the spatial quantities is

$$dm = \rho_t \, dv \tag{97}$$

By equating (96) and (97) and using the relationship defined in Eq. (93), we may define the density in the intermediate configuration as

$$\rho_g = J^e \rho_t. \tag{98}$$

Further, we define the density of the grown mass element in the material configuration as

$$\overline{\rho}_0 = \frac{dm}{dV} \tag{99}$$

which by Eqs. (90), (91), (97), and (98) can be expressed as

$$\overline{\rho}_0 = J\rho_t = J^g \rho_g \tag{100}$$

Inserting Eqs. (94) and (99) into Eq. (95) yields

$$\overline{\rho}_0 = \rho_0 + \int_{t_0}^{t} R_0 \, dt. \tag{101}$$

Eq. (101) illustrates that the density of the grown mass element is equal to the initial density and a term which takes into account the mass source.

2.4.3. *Conservation equations in growth*

Taking the time derivative of Eq. (101) will yield the local balance of mass in the material configuration:

$$\dot{\overline{\rho}}_0 = R_0 \tag{102}$$

By using the relation $\overline{\rho}_0 = J^g \rho_g$, we can write

$$\begin{aligned}\dot{\overline{\rho}}_0 = R_0 &= \frac{\partial (J^g \rho_g)}{\partial t} = \rho_g \frac{\partial J^g}{\partial t} + J^g \frac{\partial \rho_g}{\partial t} = \rho_g \left(\frac{\partial J^g}{\partial F^g_{ij}} \frac{\partial F^g_{ji}}{\partial t} \right) + J^g \frac{\partial \rho_g}{\partial t} \\ &= \rho_g J^g (F^g_{ji})^{-1} \dot{F}^g_{ji} + J^g \dot{\rho}_g = \rho_g J^g L^g_{ii} + J^g \dot{\rho}_g\end{aligned} \tag{103}$$

which may be rewritten to represent the local balance of mass in the intermediate configuration as

$$\dot{\rho}_g + \rho_g L^g_{ii} = (J^g)^{-1} R_0. \tag{104}$$

The local balance of linear momentum in the material configuration may be written (in the absence of body forces and source terms) as

$$\overline{\rho}_0 \frac{\partial v_i}{\partial t} = \frac{\partial (F_{ik} S_{kj})}{\partial x_j} \tag{105}$$

Since this work is focused on the particular case of growth under constant density, certain simplifications to the previously developed theory can be made. First, if density is kept constant then

$$\rho_0 = \rho_g = \rho \tag{106}$$

where ρ is the material's constant density. This means that the volume must change if there is a mass change. Eq. (104) can now be written as

$$R_0 = J^g \rho L^g_{ii} \tag{107}$$

Thus, if F^g_{ij} and $\dot{F}^g_{ij}$ are known, then the mass source can be directly determined.

2.4.4. *Constitutive equations in growth*

We will restrict ourselves to materials that undergo isotropic growth. An equation describing the growth which allows the calculation of the growth deformation tensor F^g must be developed. We begin with an isotropic free energy density per unit mass Ψ which is a function of the elastic right Cauchy-Green tensor C^e_{ij} and the grown material density $\overline{\rho}_0$

$$\Psi = \Psi(C^e_{ij}, \overline{\rho}_0) \tag{108}$$

Using Eqs. (83) and (84), C^e_{ij} can be rewritten as

$$C^e_{ij} = (F^g_{ki})^{-1} C_{km} (F^g_{mj})^{-1} \tag{109}$$

The time derivative of Ψ can be calculated as

$$\begin{aligned}\dot{\Psi} &= \frac{\partial \Psi}{\partial t} = \frac{\partial \Psi}{\partial C^e_{ij}} \frac{\partial C^e_{ji}}{\partial t} + \frac{\partial \Psi}{\partial \overline{\rho}_0} \frac{\partial \overline{\rho}_0}{\partial t} \\ &= \frac{\partial \Psi}{\partial C^e_{ik}} \left(\frac{\partial C^e_{km}}{\partial C_{mj}} \frac{\partial C_{ji}}{\partial t} + \frac{\partial C^e_{km}}{\partial F^g_{mj}} \frac{\partial F^g_{ji}}{\partial t} \right) + \frac{\partial \Psi}{\partial \overline{\rho}_0} \frac{\partial \overline{\rho}_0}{\partial t} \\ &= (F^g_{ik})^{-1} \frac{\partial \Psi}{\partial C^e_{km}} (F^g_{jm})^{-1} \dot{C}_{ji} - 2 C_{ik} \frac{\partial \Psi}{\partial C^e_{km}} (F^g_{jm})^{-1} (\dot{F}^g_{ji})^{-1} + \frac{\partial \Psi}{\partial \overline{\rho}_0} \dot{\rho}_0.\end{aligned} \tag{110}$$

However, since density is assumed to remain constant during growth, $\dot{\rho}_0 = 0$ and Eq. (110) becomes

$$\dot{\Psi} = (F^g_{ik})^{-1} \frac{\partial \Psi}{\partial C^e_{km}} (F^g_{jm})^{-1} \dot{C}_{ji} - 2 C_{ik} \frac{\partial \Psi}{\partial C^e_{km}} (F^g_{jm})^{-1} (\dot{F}^g_{ji})^{-1}. \tag{111}$$

A free energy density function per unit volume can be defined as

$$\Psi_0 = \rho_0 \Psi \tag{112}$$

from which the Second Piola-Kirchhoff stress is derived using

$$S_{ij} = 2 \frac{\partial \Psi_0}{\partial C_{ij}}. \tag{113}$$

The Second Piola-Kirchhoff stress corresponding to the intermediate configuration is

$$S^e_{ij} = F^g_{ik} S_{km} F^g_{jm} = 2 \frac{\partial \Psi_0}{\partial C^e_{ij}}. \tag{114}$$

Correspondingly, S_{ij} may also be calculated as

$$S_{ij} = (F^g_{ik})^{-1} S^e_{km} (F^g_{jm})^{-1}. \tag{115}$$

At this point, we can also define the Mandel Stress for the intermediate configuration, which is the work conjugate to the growth velocity gradient L^g_{ij} defined in Eq. (87), as

$$M^e_{ij} = C^e_{ik} S^e_{kj}. \tag{116}$$

The tangent modulus of the material model for growth may be calculated by using the form of S_{ij} as specified in Eq. (76) as

$$\begin{aligned}L^e_{ijkl} &= 2 \frac{\partial S^e_{ij}}{\partial C^e_{kl}} \\ &= \lambda (C^e_{ij})^{-1} (C^e_{kl})^{-1} + [\mu - \lambda \ln(J^e)][(C^e_{ik})^{-1} (C^e_{jl})^{-1} + (C^e_{il})^{-1} (C^e_{jk})^{-1}].\end{aligned} \tag{117}$$

As done previously by Lubarda and Hoger (2002) and by Kuhl (Himpel et al., 2005; Goktepe et al., 2010), the isotropic growth

deformation gradient can be defined as

$$F^g_{ij} = \upsilon \delta_{ij} \tag{118}$$

where υ is an isotropic stretch ratio due to volumetric growth and δ_{ij} is the Kronecker Delta. Using this definition, the following relations can be written:

$$J^g = \upsilon^3 \tag{119}$$

$$\overline{\rho}_0 = \upsilon^3 \rho_g \tag{120}$$

$$L^g_{ij} = \frac{\dot{\upsilon}}{\upsilon}\delta_{ij}. \tag{121}$$

Since density is assumed to remain constant during growth, Eq. (120) can be rewritten

$$\overline{\rho}_0 = \upsilon^3 \rho_0 = \upsilon^3 \rho. \tag{122}$$

The mass source term is thus

$$R_0 = J^g \rho L^g_{ii} = 3\rho\upsilon^2\dot{\upsilon}. \tag{123}$$

It can be now be seen that the mass source term is driven by the evolution of the stretch ratio due to volumetric growth and that an equation describing its evolution must be developed. Therefore, it will be assumed (see Himpel et al., 2005) that

$$\dot{\upsilon} = f(\upsilon, M^e_{ii}) \tag{124}$$

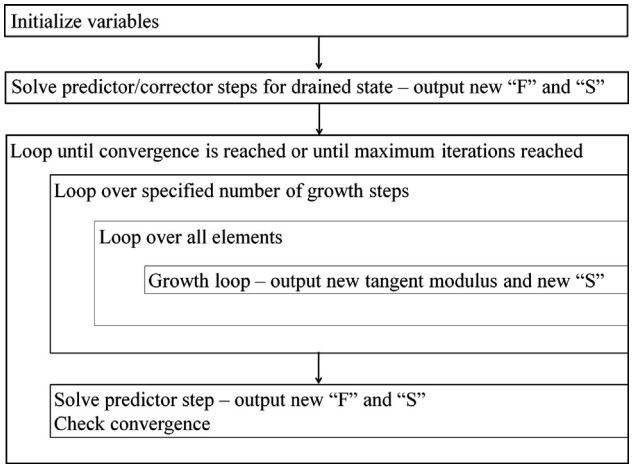

Fig. 3 – MPHETS with growth finite element implementation.

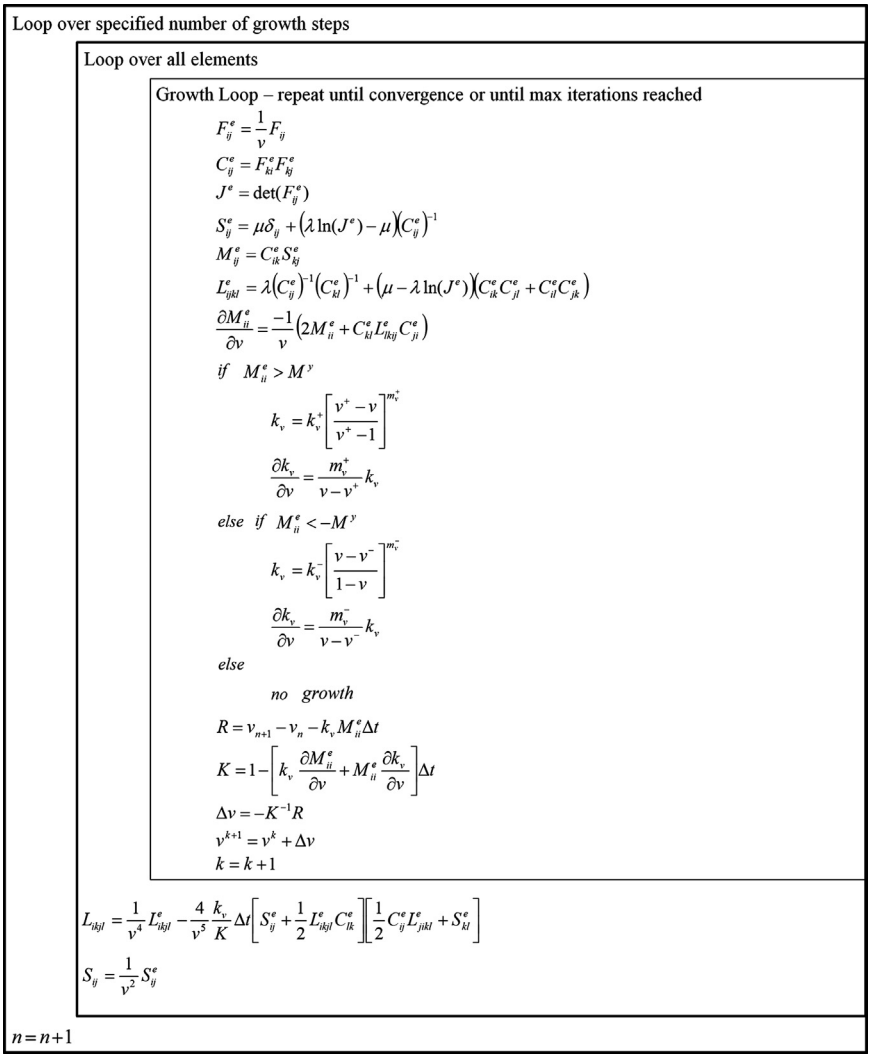

Fig. 2 – Implementation of the growth loop. Note that all Mandel stresses are calculated from the effective stress.

where the trace of the Mandel stress in the intermediate configuration provides a representative scalar value of the volumetric stress condition. The simplest form for such a function is

$$\dot{\upsilon} = k_\upsilon(\upsilon) M^e_{ii}. \tag{125}$$

In order to prevent unlimited growth, k_υ is defined as (Lubarda and Hoger, 2002; Himpel et al., 2005; Goktepe et al., 2010)

$$k_\upsilon(\upsilon) = k^+_\upsilon \left[\frac{\upsilon^+ - \upsilon}{\upsilon^+ - 1}\right]^{m^+_\upsilon} \quad \text{for } M^e_{ii} > M^y \tag{126}$$

$$k_\upsilon(\upsilon) = k^-_\upsilon \left[\frac{\upsilon - \upsilon^-}{1 - \upsilon^-}\right]^{m^-_\upsilon} \quad \text{for } M^e_{ii} < -M^y. \tag{127}$$

In Eqs. (126) and (127), the constants $\upsilon^+ > 1$ and $\upsilon^- < 1$ denote the limiting values the stretch ratio can reach due to growth and atrophy, respectively. The remaining terms (k^+_υ, m^+_υ, k^-_υ, m^-_υ) are constant material parameters which dictate how quickly the growth or atrophy of the model occurs. For the case of tensile loading, M^y is a value of the Mandel stress which represents a physiological threshold below which growth does not occur; correspondingly, once M^e exceeds M^y, growth is activated. Similar statements can be made for compression using (127).

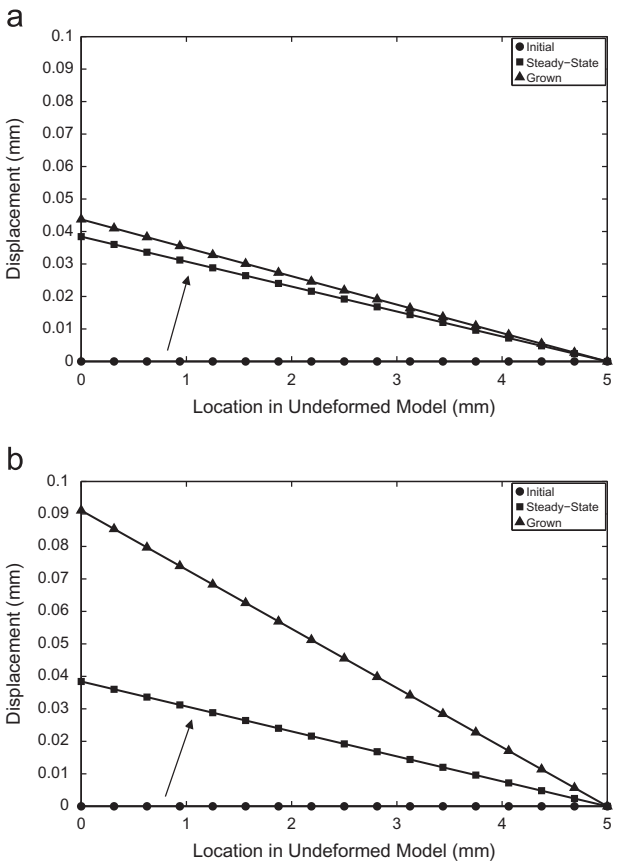

Fig. 4 – Solution variables for MPHETS confined compression problem with fluid and chemical potentials set to zero. Note that positive displacement indicates movement to the right. (a) Solid only compression problem: $k^+_\upsilon = k^-_\upsilon = 1e{-}9$. (b) Solid only compression problem: $k^+_\upsilon = k^-_\upsilon = 1e{-}8$.

2.5. *Combining MPHETS and growth*

2.5.1. *Growth finite element implementation*

In this section, the constitutive theory discussed for density preserving growth will be numerically implemented and standard finite element techniques based on an internal variable formulation for the stretch ratio will be applied. To solve the highly nonlinear governing equations for finite growth on a local level, a finite difference scheme will be

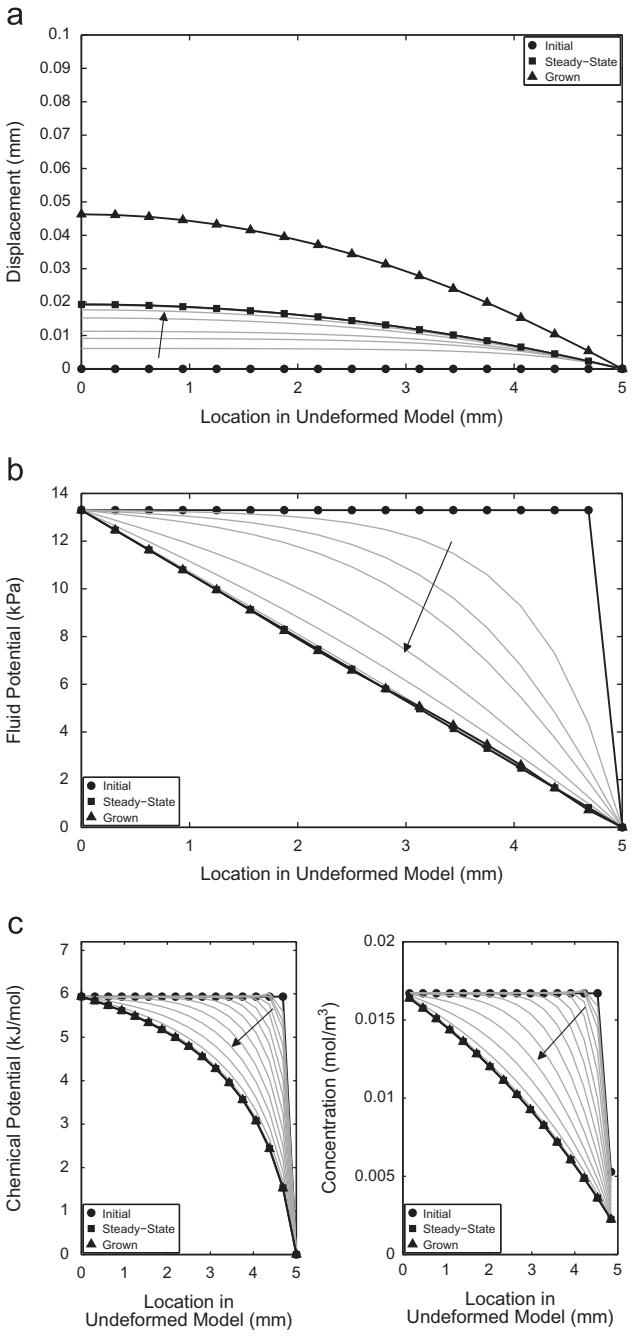

Fig. 5 – Solution fields for the MPHETS problem with growth assuming no osmosis. The gray lines indicate the time dependent MPHETS problem reaching mechanical equilibrium. (a) Time history of the displacement field. (b) Time history of the fluid potential field. (c) Time history of the chemical potential and concentration fields.

used to discretize the evolution equations (Eq. (125)) for the growth multiplier v. To numerically solve the equations on a global level, the finite element method will be used to discretize the equations for finite growth in space (Eqs. (83), (105), and (114)). This will all be done as shown in the previous literature (Himpel et al., 2005; Goktepe et al., 2010). For space limitations, we refer the reader to the afore mentioned paper for details of how the growth theory is implemented into a finite element code. We simply present here a figure briefly summarizing its details and implementation (Fig. 2). Note that the growth loop is iterated until v has converged or until the maximum number of growth steps is reached.

2.6. *Combining MPHETS and growth*

Now that the MPHETS and growth theory have been fully developed, the two must be incorporated together. To accomplish this, three key assumptions are made which are stated as follows:

(1) The rate at which growth occurs in a soft tissue (which may be on the order days, months, or even years) is significantly slower than the time required for a soft tissue to reach a drained or flowing mechanical equilibrium (which is on the order of seconds to a few hours).
(2) The stress upon which the growth loop acts is the stress in the solid skeleton, i.e. the effective stress, S^{eff}.
(3) The porosity of the porous medium remains constant during growth, i.e. any new porous media added due to growth will have the same porosity as the tissue before growth.

With these assumptions, the MPHETS and growth finite element problems will be solved as detailed in Fig. 3. First, the MPHETS problem will be solved. Again, since this is assumed to occur quickly, no growth will have yet occurred. Once this is finished, growth is allowed to occur and the growth loop (detailed in Fig. 2) is implemented. Once the growth loop finishes, the predictor step from the MPHETS problem is solved using an updated tangent modulus and effective 2nd Piola-Kirchhoff stress obtained from the growth loop. This results in a slightly modified deformation and stress state, upon which the growth loop acts again. This is repeated until convergence is reached or until some specified amount of time has passed.

3. Results

We will present two sets of results, one for a grown pure solid and another for the utilization of MPHETS and growth.

3.1. *Growth of a solid*

In this section, the fluid and chemical potentials are set to zero in the program and the resulting solid-only model is allowed to grow. The right node is fixed and a compressive stress of 100 kPa is applied to the left node. The one-dimensional domain for the problem solved was 5 mm long and contained 16 elements, each having linear shape functions for all nodal variables. The compressive load on this problem was 13.3 kPa, with all simulations using a unit cross sectional area. The effective aggregate modulus of the material was calculated from an effective Young's modulus of 100 kPa and a Poisson's ratio of 0.49. The values of v^+, v^-, k_v^+, m_v^+, k_v^-, m_v^- were assigned to be 1.3, 0.7, 1e−9, 2, 1e−9, and 3, respectively. The total growth time for all models was $t=100$ (au).

In Fig. 4(a), the steady-state solution of the MPHETS model is shown and labeled as “Steady-State”; note that at this point in the solution of the problem, no growth has yet occurred. Once the MPHETS problem is solved, then growth is allowed to occur and the model grows to the configuration labeled “Grown”. For the compression problem, the model atrophies (loses mass) and shrinks in length as shown in Fig. 4(a). The magnitude of this atrophy can be controlled by adjusting the growth constants involved in the solution. For example, if the constants k_v^+ and k_v^- are increased by one order of magnitude to 1e−8 and the same compression problem as before is solved again, the solution shown in Fig. 4(b) below is obtained. Notice that the steady-state MPHETS solutions shown in Fig. 4(b) is the same as in Fig. 4(a), however the model now exhibits significantly more atrophy.

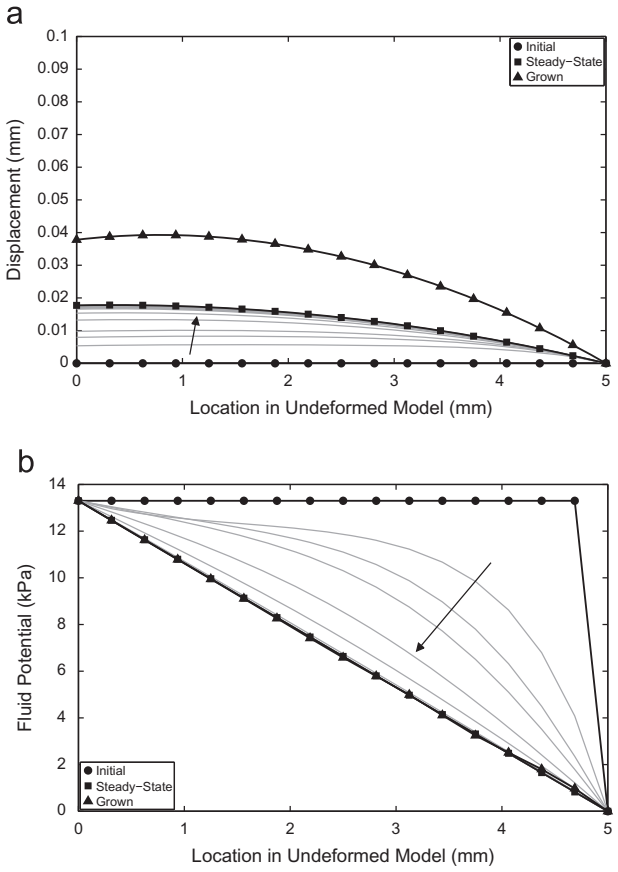

Fig. 6 – Displacement and fluid potential solutions for MPHETS confined compression with osmosis. (a) Displacement field. (b) Fluid potential field.

3.2. *Growth of a porous media*

Now the MPHETS problem with non-zero fluid and chemical potentials will be allowed to grow/atrophy and will be solved with and without osmotic effects. For these simulations, the same model geometry and values for Young's modulus and Poisson's ratio were used as in Section 3.1. The value of k_v^+ and k_v^- was 1e–8. The value of the hydraulic permeability was k_0=3.7e–12 m^4/(Ns), while the value of the convection coefficient b_{cf} was 0.8 while the value of the diffusivity d_{cc} was 4.86e–8 m^2/s. The value of both the initial porosity n_o and the activity coefficient γ^c was set to 0.5. For the case where osmosis was allowed, the value of the osmotic coefficient ϕ^c was 25. The value of the universal gas constant was R=8.31 (J/K/mol) and the temperature θ was set to 310 K. A mechanical pressure as well as a pore fluid pressure of 13.3 kPa was applied to the left hand side of the one-dimensional domain. The pore fluid pressure of the node on the far right was set to zero. The original concentration (at t=0) of all nodes except for the node on the far right was 1.67e–2 mol/m^3. The node on the far right was given an initial concentration of 1.67e–3 mol/m^3. The results for an MPHETS problem with fluid and chemical potentials present but without osmosis is shown in Fig. 5.

The results for an MPHETS problem with fluid and chemical potentials present using osmosis are shown in Figs. 6 and 7.

Notice that the steady-state MPHETS solutions of the fluid and chemical potential fields are the same as the grown solutions. This is expected since the steady-state solutions of the fluid and chemical potential fields are independent of the deformation of the solid. Since the model is in compression in both problems, Figs. 5(a) and 6(a) show that the material loses mass (atrophies) and shrinks in length as expected.

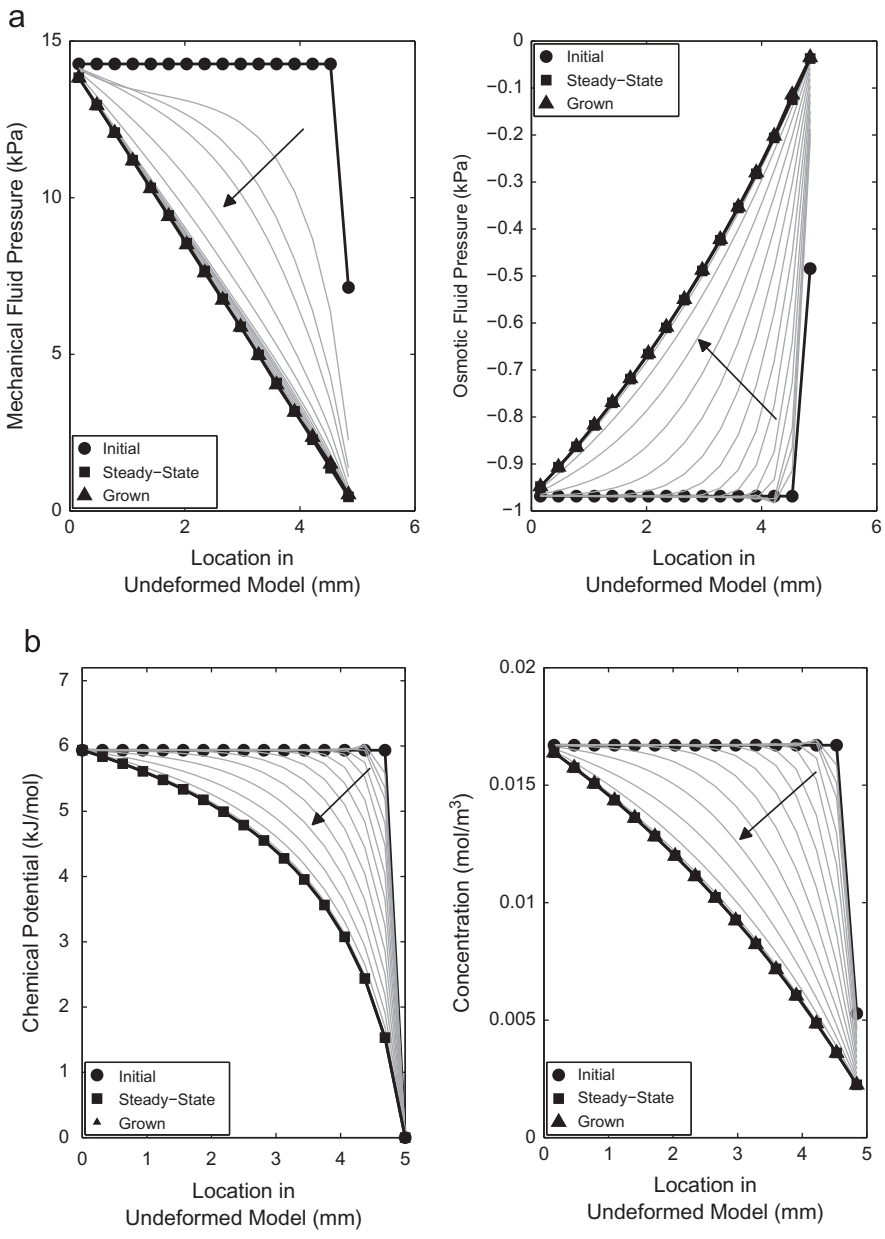

Fig. 7 – Additional solution variables in the MPHETS confined compression problem with osmosis. (a) Time history of the mechanical fluid pressure and osmotic pressure fields. (b) Time history of the chemical potential and concentration fields.

For the simulation in which osmosis is included, there is a small downward curvature in the displacement field near the left end of the model due to osmotic effects. In other words, the far left of this model displays a smaller grown displacement than that approximately 1 mm into the model from the left. This effect is due to the osmotic pressure, which has its largest magnitude near the left end of the model as can be seen in Fig. 7(a). This is in contrast to the models solved without osmosis (see Fig. 5(a)), where the largest grown displacement occurs on the far left of the model. It can also be seen that the presence of osmosis also reduces the overall peak steady state and grown displacement values. These effects are due to the complex interaction and balance of the pore fluid pressure and osmotic pressure at the left hand side of the model.

4. Discussion

When simulating a tissue without considering fluid or chemical potentials, the effective stress is equal to the total stress throughout the one-dimensional domain. In the MPHETS model, the total stress is the same in each element. However, due to the non-constant fluid potential distribution, the effective stress in each element is different. The effective stress in the left-most element (where exterior loading occurs) is near zero because the fluid potential is largest there, i.e. the fluid is taking a significant portion of the applied load in the left-most element. On the other hand, the effective stress in the right-most element is almost equal to the total stress since the fluid potential is smallest there (as imposed by a zero fluid potential boundary condition at this node). This variance in the effective stress for the MPHETS model holds significant consequences. For a one-dimensional finite element problem, we know that the total stress in each element must be equal for the model to be in equilibrium. Therefore, we can expect that each element will grow the same amount in a one-dimensional solid only problem since the effective stress is equal to the total stress in each element. With the MPHETS model, however, the effective stress varies across its length causing each element to grow a different amount.

The fact that the fluid may take a significant portion of the loading in an MPHETS model and the differential growth of each element that occurs when using an MPHETS model typically results in much smaller total deformations and total growth for a given applied stress than when using a solid only model. This is shown in Fig. 8, where the percent change in total length for a MPHETS model (with chemical potentials set to zero) as compared to that for a solid only model is plotted.

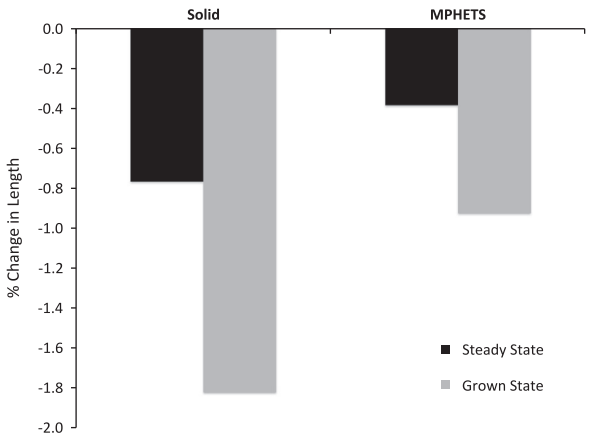

Fig. 8 – Percent change in length of FEMs implementing growth without (labeled Solid) and with (labeled MPHETS) fluid potential. This plot is a summary of the simulations described in Figs. 4(b) and 5(a). The negative values indicate that the models reduced in length.

4.1. *Limitations and future work*

There are several limitations of this work. One of the foremost simplifying assumptions is that the models considered here only grow and do not remodel. This assumption may not be applicable in certain applications since it is likely that in some diseases of interest there exist changes in volume at constant density as well as an alteration of the material property (e.g., density, strain energy) of the added tissue mass. While this is a limiting assumption, this work serves as a first step towards a working model that includes effects of both growth and remodeling. Future work in our laboratory is aimed at addressing this limitation. Another limitation of the work presented is its one dimensionality. This drawback was considered acceptable here since it is important to establish a complicated finite element model that is at first more easily interpretable. Ongoing work in our group is focused on expanding the current model into axisymmetry as well as to two and three dimensions. Finally, another limitation of this current paper is the utilization of the stress based stimuli for growth. One of the driving motivations for introducing an MPHETS model is to allow the eventual inclusion of biochemomechanical stimuli into both growth and remodeling. This is also a future goal of our research group.

4.2. *Conclusions*

In this work a finite element code was developed that simulates the growth of a one-dimensional mixed porous media mass transport swelling model undergoing finite deformations. For the assumptions made, the results demonstrate a heterogeneous growth field is achieved that is a direct result of the complex fluid–solid load distribution throughout the tissue. It was shown that significantly different amounts of growth are experienced for the same loading conditions and boundary conditions when using the MPHETS model as compared to a solid-only model. In the example including both fluid and chemical potentials, the MPHETS model experienced a marked reduction total deformation and predicted approximately 51% less growth than when not including these potentials. It is interesting to note that the inclusion of osmotic effects also altered the displacement and growth field of the simulations. This work provides the opportunity to consider more complex biochemomechanical stimuli can in the future using the described approach.

Acknowledgements

The authors would like to acknowledge Dr. Ellen Kuhl for her contributions to the present work. Funding for the present work was provided by the NIH (5R01EY020890-02 to JPVG).

REFERENCES

Almeida, E.S., Spilker, R.L., 1997. Mixed and penalty finite element models for the nonlinear behavior of biphasic soft tissues in finite deformation. Part I. Alternate formulations. Computer Methods in Biomechanics and Biomedical Engineering 1, 25–46.

Almeida, E.S., Spilker, R.L., 1998. Mixed and penalty finite element models for the nonlinear behavior of biphasic soft tissues in finite deformation. Part II. Nonlinear examples. Computer Methods in Biomechanics and Biomedical Engineering 1, 151–170.

Ambrosi, D., Ateshian, G.A., Arruda, E.M., Cowin, S.C., Dumais, J., Goriely, A., Holzapfel, G.A., Humphrey, J.D., Kemkemer, R., Kuhl, E., Olberding, J.E., Taber, L.A., Garikipati, K., 2011. Perspectives on biological growth and remodeling. Journal of Mechanics and Physics of Solids 59, 863–883.

Ambrosi, D., Mollica, F., 2002. On the mechanics of a growing tumor. International Journal of Engineering Science 40, 1297–1316.

Ateshian, G., 2007. On the theory of reactive mixtures for modeling biological growth. Biomechanics and Modeling in Mechanobiology 6, 423–445.

Biot, M.A., 1941. General theory of three-dimensional consolidation. Journal of Applied Physics 12, 155–164.

Biot, M.A., 1972. Theory of finite deformations of porous solids. Indiana Math Journal 21, 597–620.

Bowen, R., 1971a. Compressible porous-media models by the use of the theory of mixtures. International Journal of Engineering Science 20, 697–735.

Bowen, R., 1971b. Continuum theory of fluid saturated porous media. Journal of Applied Mechanics 38, 716.

Goktepe, S., Abilezb, O.J., Kuhl, E., 2010. A generic approach towards finite growth with examples of athlete's heart, cardiac dilation, and cardiac wall thickening. Journal of Mechanics and Physics of Solids 58, 1661–1680.

Gu, W.Y., Lai, W.M., Mow, V.C., 1998. A mixture theory for charged-hydrated soft tissues containing multi-electrolytes: passive transport and swelling behaviors. Journal of Biomechanical Engineering 120, 169–180.

Himpel, G., Kuhl, E., Menzel, A., Steinmann, P., 2005. Computational modelling of isotropic multiplicative growth. Computer Modeling in Engineering and Sciences 8, 119–134.

Humphrey, J.D., Rajagopal, K.R., 2002. A constrained mixture model for growth and remodeling of soft tissues. Mathematical Models and Methods in Applied Sciences 12, 407–430.

Iatridis, J.C., Laible, J.P., Krag, M.H., 2003. Influence of fixed charge density magnitude and distribution on the intervertebral disc: applications of a poroelastic and chemical electric (peace) model. Journal of Biomechanical Engineering 125, 12–24.

Kaufmann, M.V., 1996. Porohyperelastic Analysis of Large Arteries Including Species Transport and Swelling Effects. Ph.D. Dissertation, University of Arizona.

Lai, W.M., Hou, J.S., Mow, V.C., 1991. A triphasic theory for the swelling and deformation behaviors of articular cartilage. Journal of Biomechanical Engineering 113, 245–258.

Lee, E.H., 1969. Elastic–plastic deformation at finite strains. Journal of Applied Mechanics 36, 1.

Levenston, M.E., Frank, E.H., Grodzinsky, A.J., 1998. Variationally derived 3-field finite element formulations for quasistatic poroelastic analysis of hydrated biological tissues. Computer Methods in Applied Mechanics and Engineering 156, 231–246.

Lubarda, V.A., Hoger, A., 2002. On the mechanics of solids with a growing mass. International Journal of Solids and Structures 39, 4627–4664.

Rodriguez, E.K., Hoger, M.A., 1994. Stress-dependent finite growth in soft elastic tissues. Journal of Biomechanics 27, 455–467.

Simon, B.R., Kaufman, M.V., Liu, J., Baldwin, A.L., 1998a. Porohyperelastic-transport-swelling theory, material properties and finite element models for large arteries. International Journal of Solids and Structures 35, 5021–5031.

Simon, B.R., Kaufmann, M.V., McAfee, M.A., Baldwin, A.L., 1998b. Porohyperelastic finite element analysis of large arteries using abaqus. Journal of Biomechanical Engineering 120, 296–298.

Spilker, R.L., Suh, J.K., Mow, V.C., 1992. A finite element analysis of the indentation stress–relaxation response of linear biphasic articular cartilage. Journal of Biomechanical Engineering 114, 191–201.

Vande Geest, J.P., Simon, B.R., Rigby, P.H., Newberg, T.P., 2011. Coupled porohyperelastic mass transport (phexpt) finite element models for soft tissues using abaqus. Journal of Biomechanical Engineering 133, 044502.